



Visualization of Discontinuous Vector Field Topology

Egzon Miftari , Daniel Durstewitz , and Filip Sadlo 

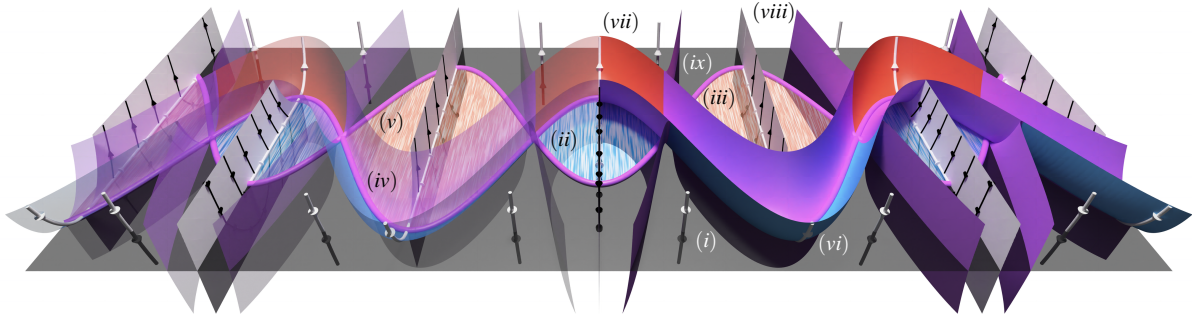


Fig. 1: Discontinuity (horizontal semitransparent plane) separating upper from lower continuous flow part, and exhibiting crossing flow (i) (gray) where streamsets are 1-manifold (white lines) in both parts, attracting sliding flow (ii) (blue LIC texture) and repelling sliding flow (iii) (red LIC) where streamsets are 2-manifold (white surfaces) in both parts. Such sliding flow is bounded by inbound (iv) or outbound (v) boundary switch curves (violet lines) or domain boundaries. Inbound boundary switch curves give rise to stable (vi) (blue) and unstable (vii) (red) manifolds that separate 1-manifold streamsets of qualitatively different flow behavior, as well as equitrices (viii) (violet surfaces), that separate 1-manifold streamsets (i) from not 1-manifold streamsets (ix). Notice that streamsets can change their dimensionality between 1-manifold and 2-manifold at the inbound boundary switch curves.

Abstract—This paper extends the concept and the visualization of vector field topology to vector fields with discontinuities. We address the non-uniqueness of flow in such fields by introduction of a time-reversible concept of equivalence. This concept generalizes streamlines to streamsets and thus vector field topology to discontinuous vector fields in terms of invariant streamsets. We identify respective novel critical structures as well as their manifolds, investigate their interplay with traditional vector field topology, and detail the application and interpretation of our approach using specifically designed synthetic cases and a simulated case from physics.

Index Terms—Discontinuous vector field topology, equivalence in non-unique flow, non-smooth dynamical systems

1 INTRODUCTION

Vector fields are a fundamental tool for understanding and modeling of a wide field of problems in science and engineering. Being motivated by physically continuous settings, such as electric, magnetic, and flow fields, vector fields are predominantly used in smooth formulation. Also in case of discretized data, e.g., originating from numerical simulation, continuity is typically established by interpolation for their (visual) analysis.

Many mathematical problems and phase spaces of physical problems, however, exhibit discontinuities. For example, a mathematical description can be partitioned into a set of piecewise continuous vector fields that meet in a discontinuous manner. In physics, the phase space of problems including, e.g., friction and stiction can exhibit lower-dimensional manifolds across which the otherwise continuous vector field is discontinuous.

Vector field topology [8, 9] is predominantly employed in terms of

- Egzon Miftari is with Heidelberg University. E-mail: egzon.miftari@iwr.uni-heidelberg.de.
- Daniel Durstewitz is with Heidelberg University. E-mail: daniel.durstewitz@zi-mannheim.de.
- Filip Sadlo is with Heidelberg University. E-mail: sadlo@uni-heidelberg.de.

Manuscript received xx xxx. 201x; accepted xx xxx. 201x. Date of Publication xx xxx. 201x; date of current version xx xxx. 201x. For information on obtaining reprints of this article, please send e-mail to: reprints@ieee.org. Digital Object Identifier: xx.xxx/TVCG.201x.xxxxxx

critical points (isolated zeros of the vector field), separatrices (streamlines that converge to saddle-type critical points or periodic orbits in forward or reverse time), and periodic orbits (isolated closed streamlines). It has proven particularly useful for analyzing vector fields by providing a concise qualitative representation of their overall transport.

However, although mathematical research is being conducted on transport in discontinuous vector fields, the vector field topology concept has not yet been extended accordingly. It is therefore the aim of this work to fill this gap by formulating a vector field topology for discontinuous vector fields. On the one hand, the presence of discontinuities impacts streamline (invariant manifold) geometry and thus affects traditional and causes novel topological structures. On the other hand, the discontinuities can also cause transition of the dimensionality of invariant manifolds, including breaking of transport reversibility. This motivates us to reinterpret invariant manifolds in terms of equivalence classes, and this way generalize vector field topology to discontinuous flow and possibly beyond.

The contributions of this work include:

- generalization of vector field topology to discontinuous flow,
- by providing a theory on time-reversible flow equivalence, and
- introduction of manifolds delineating transport equivalence.

2 RELATED WORK

Vector field topology has been introduced in the field of scientific visualization by Helman and Hesselink [8, 9]. Various extensions have been proposed since then, including saddle connectors [21], boundary switch curves [23], uncertainty [19], time-dependency [11, 12], higher

order [20], and higher dimensions [10]. A good introduction to the topic is provided by Asimov [2].

An overview and introduction on non-smooth dynamical systems is provided by Glendinning et al. [7]. The authors report the history and critical findings in the context of non-smooth maps and vector fields. The mathematical foundation and solution theory was first laid out by Filippov et al. [6]. There are many phenomena unique to discontinuous systems, like two-fold singularities at the intersection of two boundary switch curves, or hidden dynamics contained inside a discontinuity. The structural stability of two-fold singularities has been, among others, studied by Fernández-García et al. [5]. Hidden dynamics of flows with discontinuities have been investigated by Jeffrey et al. [13, 14, 16].

The generalization of continuous flows and initial value problems to discontinuous flows and differential inclusions has led to different generalization approaches. Considering this, closely related to our work are the multiflows of Thieme [22], which are defined through relations instead of equivalency relations and only for forward time. Ball [3] introduced the generalized semiflow, which consists of a family of maps called “solutions” and is also only defined in forward time direction. Lastly, there is the multi-valued semiflow of Melnik and Valero [18]. Here, the main difference between the multi-valued flow to our approach is the relaxation of the image of the flow as a group action, whereas the multi-valued flow only requires inclusion instead of equality of the concatenation of flow maps. All of these approaches are conceptually similar, but do not focus on reversibility of the transport and thus do not generalize vector field topology.

3 FUNDAMENTALS

Since streamlines are the fundamental concept in vector field topology, we first discuss continuous dynamical systems and their initial value problems (Section 3.1). We then treat traditional (continuous) vector field topology in terms of invariant sets (Section 3.2), followed by an introduction to piecewise continuous dynamical systems (Section 3.3).

3.1 Continuous Dynamical Systems

In this work, we consider steady (time-independent) vector fields $\mathbf{u}(\mathbf{x}) \in \mathbb{R}^n$, with $\mathbf{x} \in \Omega$ in n -dimensional domain $\Omega \subseteq \mathbb{R}^n$ and $n = 2, 3$. Here, we require $\mathbf{u}(\mathbf{x})$ to be at least Lipschitz continuous. Later on (Section 3.3), we will require this only in a piecewise manner. For brevity, we write, e.g., \mathbf{u} for $\mathbf{u}(\mathbf{x})$, where unambiguous.

For Lipschitz continuous \mathbf{u} , the initial value problem (IVP)

$$\dot{\mathbf{x}}(t) = \mathbf{u}(\mathbf{x}(t)), \quad \mathbf{x}(0) = \mathbf{x}_0 \quad (1)$$

has a guaranteed and unique (Picard–Lindelöf) solution $\mathbf{x}(t)$ for arbitrary initial value \mathbf{x}_0 and integration time t , which is also termed *streamline*. Such advection-based description of a dynamical system (also denoted vector field) is referred to as *flow* of a vector field, and portrays the movement of “massless particles”. For each IVP, we can define the mapping $\boldsymbol{\varphi} : \Omega \times \mathbb{R} \rightarrow \Omega$ with

$$\boldsymbol{\varphi}(\mathbf{x}_0, t) := \mathbf{x}(t), \quad (2)$$

which relates an initial position \mathbf{x}_0 to the advected position $\mathbf{x}(t)$ after advection time t , and is denoted *flow map*. Often, the notation $\boldsymbol{\varphi}_t(\mathbf{x}) := \boldsymbol{\varphi}(\mathbf{x}, t)$ is used to make the flow implicit, with emphasis on the action of the mapping $\boldsymbol{\varphi}_t(\mathbf{x})$ on Ω . This action is, in fact, a group action of the group (\mathcal{P}, \circ) on Ω , with $\mathcal{P} = \{\boldsymbol{\varphi}_t | t \in \mathbb{R}\}$ being the collection of flow maps and \circ representing map composition. One can easily verify that the group properties (identity, associativity, and inverse element) hold, and that it is homomorphic to the additive group on the real numbers (we will rely on this when deriving equivalence sets below).

3.2 Continuous Vector Field Topology

Topology, in contrast to geometry, is only concerned with properties of a mathematical object that are invariant under continuous deformations of the object. In the context of dynamical systems and flows, we are concerned with structural stability, as described by Andronov and

Pontryagin [1]. There are many different types of structural stability (e.g., linear, asymptotic, weak, etc.). *Invariant sets*

$$\mathcal{I} = \boldsymbol{\varphi}_t(\mathcal{I}), \quad \forall t \in \mathbb{R}, \quad (3)$$

which are sets that are closed under the action of $\boldsymbol{\varphi}_t$, play a pivotal role in analyzing the stability of a dynamical system with respect to small perturbations. Notice that any streamline with $t \rightarrow \pm\infty$ is an invariant set, and therefore a basic concept in vector field topology termed *invariant manifold*.

Particularly important for stability analysis are distinguished invariant sets, such as *critical points* \mathbf{x}_c with

$$\mathbf{u}(\mathbf{x}_c) = \mathbf{0}, \quad \mathbf{x}_c \equiv \mathbf{x}(t), \quad \forall t \in \mathbb{R}, \quad (4)$$

at which the vector field exhibits a zero vector, and which therefore constitute their own invariant set. Critical points have to be isolated ($\det \nabla \mathbf{u}(\mathbf{x}_c) \neq 0$), and are structurally stable if all eigenvalues of $\nabla \mathbf{u}(\mathbf{x}_c)$ have nonzero real part. They can be classified into rotating (complex eigenvalues) and non-rotating (real eigenvalues), as well as inflow (negative real parts, also denoted *stable*) and outflow (positive real parts, also denoted *unstable*). For example, a source has real positive eigenvalues, a spiral sink complex eigenvalues with negative real parts, and saddles have at least one negative and at least one positive real part. The corresponding directions of inflow (convergence to \mathbf{x}_c in forward time) and outflow (convergence to \mathbf{x}_c in reverse time) are identified by the respective eigenvectors. In case of saddles, the invariant sets seeded at \mathbf{x}_c along these directions are denoted *separatrices* (or *stable/unstable manifolds*), which separate the domain into regions of qualitatively different flow behavior, since in continuous vector fields, flow cannot cross these separatrices. In 3D flow, saddles exhibit a two-dimensional separatrix “spanned” by the two eigenvectors with equal-sign real parts, and a one-dimensional separatrix in direction of the remaining eigenvector.

A further type of distinguished invariant set (critical structure) in 3D vector fields are *periodic orbits*

$$\mathbf{x}(t) = \mathbf{x}(t + kT), \quad \forall t \in \mathbb{R}, \forall k \in \mathbb{Z}, \quad (5)$$

with $\mathbf{u}(\mathbf{x}(t)) \neq \mathbf{0}$, and period $T \in \mathbb{R} \setminus \{0\}$. Periodic orbits are classified by means of the Poincaré map $\boldsymbol{\pi} : \mathcal{S} \rightarrow \mathcal{S}$ with $\mathcal{S} \subset \mathbb{R}^2$, also called first-recurrence map. The Poincaré map is defined on the Poincaré section \mathcal{S} , a section through $\mathbf{x}(t)$ for a chosen t and oriented transversal to $\mathbf{u}(\mathbf{x}(t))$. \mathcal{S} is chosen small enough such that streamlines seeded on it intersect it only after a full revolution, not after a half one. In other words, if \mathbf{n} is the normal of \mathcal{S} and $\boldsymbol{\xi} \in \mathcal{S}$, then $\mathbf{u}(\boldsymbol{\gamma}(\boldsymbol{\xi})) \cdot \mathbf{n}$ has the same sign as $\mathbf{u}(\boldsymbol{\varphi}(\boldsymbol{\gamma}(\boldsymbol{\xi}), t_i)) \cdot \mathbf{n}$, assuming that the streamline intersects \mathcal{S} after time t_i and that $\boldsymbol{\gamma}$ transforms coordinates from \mathcal{S} to Ω . This way, the Poincaré map

$$\boldsymbol{\pi}(\boldsymbol{\xi}) = \boldsymbol{\gamma}^{-1}(\boldsymbol{\varphi}(\boldsymbol{\gamma}(\boldsymbol{\xi}), t_i)) \quad (6)$$

maps streamlines seeded at $\boldsymbol{\xi} \in \mathcal{S}$ to that next intersection between the streamline and \mathcal{S} . Periodic orbits are structurally stable if both eigenvalues of $\nabla \boldsymbol{\pi}(\boldsymbol{\xi}_p)$ (with $\boldsymbol{\xi}_p$ on the orbit) are off the complex unit circle. Eigenvalues outside the complex unit circle indicate unstable (outflow) behavior from the orbit, whereas those inside the complex unit circle indicate stable (inflow) behavior toward the orbit. Saddle-type periodic orbits have one eigenvalue inside and one eigenvalue outside the complex unit circle, and the invariant sets (streamsheets) seeded along the corresponding eigenvectors again give rise to separatrices that separate the domain into regions of qualitative different flow. In this case, both separatrices are two-dimensional. Further details can be found, e.g., in the introduction by Asimov [2].

We will see below, that in contrast to traditional (continuous) vector field topology, where separatrices are caused only by saddle-type critical structures, separatrices can also be caused by discontinuities, and by separatrices of lower-dimensional flow “within” discontinuities.

In flow visualization, it is common to color stable manifolds blue (indicating convergence to \mathbf{x}_c), and unstable ones red. As we will see in this work, discontinuities can also cause separatrices due to their attracting and repelling properties. In that sense, they can act as critical structures, and we color the attracting blue and the repelling red.

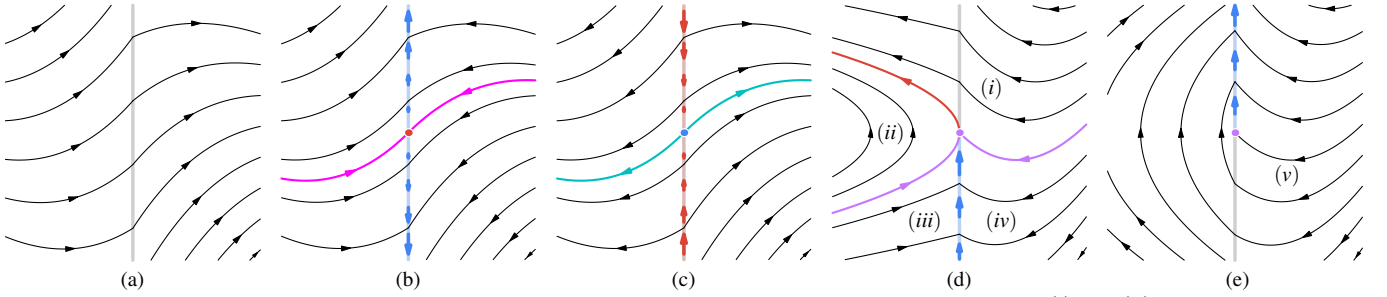


Fig. 2: Piecewise continuous flow with discontinuity Σ_{ij} (gray). 1-manifold streamsets (black) in (a) and at (i) and (ii) in (d). All other black lines represent streamsets that are not 1-manifold. (a) 1D crossing flow (on Σ_{ij}) exhibits C^0 continuous streamlines at Σ_{ij} . (b) 1D attracting sliding flow (blue) with source (red point), and stable streamset manifolds (magenta) separating streamsets in 2D flow. (c) 1D repelling sliding flow with sink (opposite to (b)). (d) Inbound boundary switch flow on the left, with boundary switch point (violet point), attracting sliding flow (blue), unstable manifold (red) separating 1-manifold streamsets, and equitrices (violet lines) separating 1-manifold streamsets ((i),(ii)) from not 1-manifold streamsets ((iii),(iv)). (e) Outbound boundary switch flow (left) with boundary switch point does neither create separating streamset manifolds nor equitrices (streamset (v) does not separate). Remaining cases by flow reversal and swapping of red/blue and magenta/cyan.

3.3 Discontinuous Dynamical Systems

Discontinuities in dynamical systems are typically present as codimension-1 manifolds, for example, because n -dimensional continuous vector field parts meet at their $(n-1)$ -dimensional boundaries, or in other words, along their codimension-1 boundaries. Since such discontinuities locally separate n -dimensional space into two parts, the vector field has at least two non-agreeing limits at each point of the discontinuity, induced by the two involved vector field parts. Dynamical systems with discontinuities on codimension- k manifolds with $k > 1$, are per se not feasible, because such manifolds cannot separate n -dimensional space and thus, due to continuity of the vector field in the “remaining space around” the discontinuity, the limit from all these directions would be identical, which would result in C^0 continuity at the “discontinuity”. Notice that C^0 continuity is widely present in vector fields in practice (e.g., due to tensor-product linear interpolation of discretized data) and does not overly affect streamlines.

As a consequence, discontinuous vector field topology has to focus on codimension-1 discontinuities across which the vector field “jumps”. For practical reasons, we assume the discontinuities to represent piecewise smooth manifolds.

Let the piecewise continuous vector field $\mathbf{u}(\mathbf{x})$ be

$$\mathbf{u}(\mathbf{x}) = \mathbf{u}_i(\mathbf{x}), \quad \mathbf{x} \in \Omega_i, \quad (7)$$

$$\Omega = \bigcup_i \bar{\Omega}_i, \quad \{\} = \bigcap_i \Omega_i, \quad (8)$$

$$\Sigma_{ij} = \bar{\Omega}_i \cap \bar{\Omega}_j, \quad i \neq j, \quad (9)$$

with partition $\bar{\Omega}_i$ of Ω , closure $\bar{\Omega}_i := \Omega_i \cup \partial\Omega_i$ with boundary $\partial\Omega_i$, discontinuity manifolds Σ_{ij} (of codimension 1), and at least Lipschitz continuous vector field parts \mathbf{u}_i . Notice that from now on, we use the symbol \mathbf{u} also for *only piecewise* continuous dynamical systems.

Following the seminal work by Filippov [6], a generalization of ordinary differential equations to piecewise continuous dynamical systems \mathbf{u} is termed *differential inclusion*

$$\dot{\mathbf{x}}(t) \in \mathbf{u}(\mathbf{x}(t)), \quad \mathbf{x}(0) = \mathbf{x}_0, \quad (10)$$

$$\mathbf{u}(\mathbf{x}) = \begin{cases} \mathbf{u}_i(\mathbf{x}) & \text{if } \mathbf{x} \in \Omega_i, \\ C(\{\mathbf{u}_i(\mathbf{x}), \mathbf{u}_j(\mathbf{x})\}) & \text{if } \mathbf{x} \in \Sigma_{ij}, \end{cases} \quad (11)$$

with $C(\mathcal{A})$ being the convex hull of set \mathcal{A} , i.e., consisting of all convex combinations of all $a_k \in \mathcal{A}$. Since, in general, $\mathbf{u}_i(\mathbf{x}) \neq \mathbf{u}_j(\mathbf{x})$ for $\mathbf{x} \in \Sigma_{ij}$, $C(\{\mathbf{u}_i(\mathbf{x}), \mathbf{u}_j(\mathbf{x})\})$ is a set, and thus $\mathbf{u}(\mathbf{x})$ is an upper semicontinuous [6] set-valued map. As a consequence, solutions to Equation 10 are absolutely continuous [6] functions $\mathbf{x}(t)$ satisfying $\dot{\mathbf{x}}(t) \in \mathbf{u}(\mathbf{x}(t))$ almost everywhere. By applying the transformation $t \mapsto -t$, we obtain the time-reversed system $\dot{\mathbf{x}}(t) \in -\mathbf{u}(\mathbf{x}(t))$, with $-\mathbf{u}(\mathbf{x}(t))$ being also upper semicontinuous, and therefore this systems

indeed describes the flow in reverse time. We want to remark that the usage of the convex hull in this definition complies with Filippov [6] and can be expressed in terms of linear combinations. Nevertheless, there exist relaxations of this property to nonlinear combinations by Jeffrey et al. [7, 14–16], which we do not cover in this work.

3.3.1 Crossing and Sliding Flow

The flow of the piecewise continuous $\mathbf{u}(\mathbf{x})$ is well defined in the parts Ω_i , but its set-valued property (Equation 11) on Σ_{ij} has implications on the flow. Let $\mathbf{n}_{ij}(\mathbf{x})$, $\mathbf{x} \in \Sigma_{ij}$ be the normal of Σ_{ij} and point from Σ_{ij} into Ω_j . With this normal, $\mathbf{u}(\mathbf{x})$ at points $\mathbf{x} \in \Sigma_{ij}$ can be classified into three fundamental cases:

Crossing flow (Figure 2a) is present if

$$(\mathbf{u}_i(\mathbf{x}) \cdot \mathbf{n}_{ij}(\mathbf{x}))(\mathbf{u}_j(\mathbf{x}) \cdot \mathbf{n}_{ij}(\mathbf{x})) > 0. \quad (12)$$

Due to the linear combinations of $\mathbf{u}_i(\mathbf{x})$ and $\mathbf{u}_j(\mathbf{x})$ (Equation 11), the entire set $\mathbf{u}(\mathbf{x})$ at $\mathbf{x} \in \Sigma_{ij}$ points from Ω_i to Ω_j in this configuration. And since Σ_{ij} is a null set, integration of an IVP through Σ_{ij} is not affected by Σ_{ij} with respect to topological considerations. That is, the resulting streamline crosses Σ_{ij} at \mathbf{x} and is C^0 continuous there.

Attracting sliding flow (Figure 2b) is present if

$$(\mathbf{u}_i(\mathbf{x}) \cdot \mathbf{n}_{ij}(\mathbf{x}))(\mathbf{u}_j(\mathbf{x}) \cdot \mathbf{n}_{ij}(\mathbf{x})) < 0 \wedge \mathbf{u}_i(\mathbf{x}) \cdot \mathbf{n}_{ij}(\mathbf{x}) > 0. \quad (13)$$

Here, the entire set of linear combinations $\mathbf{u}(\mathbf{x})$ at $\mathbf{x} \in \Sigma_{ij}$ points toward Σ_{ij} . That is, an IVP passing through this point cannot escape Σ_{ij} and keeps *sliding* inside Σ_{ij} (see blue arrows) as long as the flow stays in this attracting configuration. This sliding can be formulated by requiring the normal component of the linear combinations to vanish:

$$(\lambda \mathbf{u}_i(\mathbf{x}) + (1 - \lambda) \mathbf{u}_j(\mathbf{x})) \cdot \mathbf{n}_{ij} = 0, \quad (14)$$

with $\lambda \in [0, 1]$. Solving for λ provides the attracting sliding flow

$$\bar{\mathbf{u}}(\mathbf{x}) = \frac{\mathbf{n}_{ij} \times (\mathbf{u}_j(\mathbf{x}) \times \mathbf{u}_i(\mathbf{x}))}{(\mathbf{u}_i(\mathbf{x}) - \mathbf{u}_j(\mathbf{x})) \cdot \mathbf{n}_{ij}} \quad \text{on } \Sigma_{ij}. \quad (15)$$

From the continuity of \mathbf{u}_i within Ω_i and \mathbf{u}_j within Ω_j follows that $\bar{\mathbf{u}}$ is continuous within Σ_{ij} .

Finally, *repelling sliding flow* (Figure 2c) is present if

$$(\mathbf{u}_i(\mathbf{x}) \cdot \mathbf{n}_{ij}(\mathbf{x}))(\mathbf{u}_j(\mathbf{x}) \cdot \mathbf{n}_{ij}(\mathbf{x})) < 0 \wedge \mathbf{u}_i(\mathbf{x}) \cdot \mathbf{n}_{ij}(\mathbf{x}) < 0. \quad (16)$$

In these configurations, the set of linear combinations $\mathbf{u}(\mathbf{x})$ at $\mathbf{x} \in \Sigma_{ij}$ consists of directions pointing away from Σ_{ij} , and additionally of a single direction pointing along Σ_{ij} (which can also be determined according to Equation 15). Thus, solutions may leave the discontinuity at any point, but are also allowed to slide along Σ_{ij} . This means, that IVP solutions passing a point $\mathbf{x} \in \Sigma_{ij}$ of repelling sliding flow are not unique and one has to consider a set of possible solutions. Notice that due to the discussed time reversibility, attracting sliding flow faces the same non-uniqueness issue for reverse IVPs, as time reversal transforms attracting sliding flow to repelling sliding flow, and vice versa.

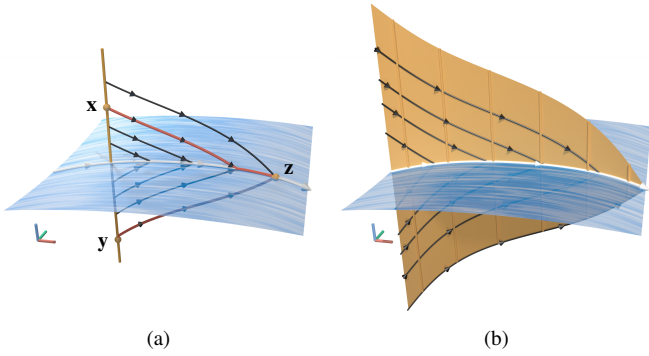


Fig. 3: Attracting sliding flow $\bar{\mathbf{u}}$ (blue LIC [4]) on discontinuity Σ_{ij} . (a) Equivalence class $[\mathbf{x}] (= [\mathbf{y}])$ (orange curve) with points \mathbf{x} and \mathbf{y} (orange dots) and $\boldsymbol{\varphi}_t(\mathbf{x}) = \boldsymbol{\varphi}_t(\mathbf{y}) = \mathbf{z}$, and some involved initial value problems (black). (b) Streamset $\tilde{\mathbf{x}}(t)$ (orange surface) of equivalence class $[\mathbf{x}]$ from (a). Orange lines are equivalence classes, and at the same time represent isotemporal sections (timelines) of streamset $\tilde{\mathbf{x}}(t)$. In all figures, x -axis is colored red, y -axis green, and z -axis blue.

4 METHOD

The non-uniqueness of reversible IVP solutions that are in contact with attracting sliding flow or repelling sliding flow has a major impact on traditional topological structures, and also causes novel topological structures. Based on equivalence classes, we propose to treat these non-unique solutions as invariant sets with possibly non-manifold geometry. As a consequence, solutions can intersect, causing novel phenomena in vector field topology.

4.1 Equivalence and Invariant Sets

Piecewise continuous dynamical systems differ from continuous dynamical systems in the important fact that their IVP solutions can violate the flow map group properties from Section 3.1. In fact, for $\boldsymbol{\varphi}_t$ with $t \in \mathbb{R}$, and thus negative t representing solutions of the time-reversed system, the inverse element property $\boldsymbol{\varphi}_t \circ \boldsymbol{\varphi}_{-t} = \text{id}_{\Omega}$ does not hold for solutions containing (attracting or repelling) sliding flow. The reason is that such inverse element relation needs to integrate forth and back, and thus becomes non-unique both in attracting and repelling sliding flow. There have been many different attempts to conserve the group characterization of the flow map, including multiflow [22] (only in forward time) and others [3, 18]. Since the main reason for the violation of the group properties is that the flow map now can map points non-uniquely to sets instead of uniquely points to points, we propose to abandon traditional IVP solutions (streamlines) as the basic building block in transport (and topology) and instead include the set-valued characteristic of Equation 11.

First, let us define the equivalence relation (red paths in Figure 3a)

$$\mathbf{x} \sim \mathbf{y} \Leftrightarrow \exists t \in \mathbb{R} : \mathbf{y} \in \boldsymbol{\varphi}_t^{-1}(\boldsymbol{\varphi}_t(\mathbf{x})), \quad \mathbf{x}, \mathbf{y} \in \Omega, \quad (17)$$

where $\boldsymbol{\varphi}_t^{-1}$ denotes the preimage of the flow map $\boldsymbol{\varphi}_t(\mathbf{x})$ (notice that $\boldsymbol{\varphi}_t(\mathbf{x})$ can be a set of points due to the non-uniqueness from Equation 11). With this, we can define the equivalence class

$$[\mathbf{x}] := \{\mathbf{y} \in \Omega \mid \mathbf{y} \sim \mathbf{x}\}. \quad (18)$$

It is easy to prove that \sim is indeed an equivalence relation and that each class $[\mathbf{x}]$ contains all points of equivalent initial conditions, i.e., those initial points that can result in the same point. See the orange curve in Figure 3a for an example for $[\mathbf{x}]$. With this, we obtain the quotient set

$$\Omega/\sim := \{[\mathbf{x}] \mid \mathbf{x} \in \Omega\}. \quad (19)$$

Notice that Ω/\sim is in fact a topological space if we equip it with the quotient topology. We can now extend the flow map to this quotient set by means of the *equivalence flow map* $\tilde{\boldsymbol{\varphi}}_t : \Omega/\sim \times \mathbb{R} \rightarrow \Omega/\sim$ with

$$\tilde{\boldsymbol{\varphi}}_t([\mathbf{x}]) := \{\boldsymbol{\varphi}_t(\mathbf{y}) \mid \mathbf{y} \sim \mathbf{x}\}, \quad (20)$$

which maps equivalence classes to equivalence classes with time-reversal consistency. This is a group action of the group (\mathcal{P}, \circ) on Ω/\sim , with

$$\tilde{\mathcal{P}} = \{\tilde{\boldsymbol{\varphi}}_t \mid t \in \mathbb{R}\}. \quad (21)$$

That is, $\tilde{\boldsymbol{\varphi}}_t \circ \tilde{\boldsymbol{\varphi}}_{-t}(\mathbf{x}) = \text{id}_{\Omega/\sim}$ holds now.

With this, we can define the *equivalence streamset* $\tilde{\mathbf{x}}(t)$, the counterpart to a streamline for piecewise continuous dynamical systems

$$\tilde{\mathbf{x}}(t) := \tilde{\boldsymbol{\varphi}}_t([\mathbf{x}_0]), \quad \tilde{\mathbf{x}}(0) = [\mathbf{x}_0]. \quad (22)$$

Equivalence streamsets represent invariant sets in piecewise continuous flow, and are the basic building block in discontinuous vector field topology, replacing the role of streamlines in traditional vector field topology. Notice that equivalence streamsets generalize streamlines, i.e., they are identical to streamlines in continuous flow, and thus our discontinuous topology generalizes traditional vector field topology.

Notice that equivalence streamsets $\tilde{\mathbf{x}}(t)$ are defined on Ω/\sim . Accordingly, any ‘‘timeline’’ $\tilde{\mathbf{x}}(t)$ for a given t is an equivalence set, too (see orange lines in Figure 3b). Equivalence streamsets (which we also denote streamsets from now on for brevity) can maintain their dimensionality when crossing discontinuities Σ_{ij} , but can also undergo dimensionality transition. For example, in Figure 6a the white streamset is a surface on the left side and turns into a line at the boundary of the discontinuity. Contrary, in Figure 6b, the streamset is a line on the right side and turns into a surface at the boundary of the discontinuity.

4.2 Critical Structures and Separatrices

As we have seen above, *critical structures* (consisting of critical points and periodic orbits in continuous vector fields) are derived for continuous vector fields by means of distinguished invariant sets in terms of streamlines. Consequently, we formulate critical structures for piecewise continuous vector fields by means of distinguished invariant sets in terms of streamsets. Critical points (Equation 4) in terms of streamsets are identical to traditional critical points, also in piecewise continuous vector fields, because stationary equivalence classes would require entire manifolds with $\mathbf{u}([\mathbf{x}]) = \mathbf{0}$, which is considered degenerate in topological analysis. Periodic orbits in terms of streamsets

$$\tilde{\mathbf{x}}(t) = \tilde{\mathbf{x}}(t + kT), \quad \forall t \in \mathbb{R}, \forall k \in \mathbb{Z}, \quad (23)$$

with $\mathbf{u}(\mathbf{x}) \neq \mathbf{0}, \forall \mathbf{x} \in \tilde{\mathbf{x}}(t)$, and period $T \in \mathbb{R} \setminus \{0\}$, on the other hand, include 1-manifold (traditional) periodic orbits, but additionally, for piecewise continuous vector fields, streamsets that are not 1-manifold.

As it turns out, traditional critical points and periodic orbits need to be extracted from Ω (Section 4.2.1), as well as from the sliding flow $\bar{\mathbf{u}}$ on the Σ_{ij} (Section 4.2.2). Novel discontinuity-induced structures are covered in Section 4.2.3. Finally, separatrices caused by these traditional and novel structures can experience bypassing when reaching sliding flow, as discussed in Section 4.2.4.

4.2.1 Traditional Critical Structures within n D Space

In piecewise continuous vector fields, critical points and periodic orbits can exist within an Ω_i , or in case of periodic orbits, can also extend through discontinuities with crossing flow (sliding flow could turn a periodic orbit into a streamset that is not 1-manifold and potentially into a periodic streamset according to Equation 23). Thus, traditional critical points and periodic orbits have to be extracted also from piecewise continuous n D flow. As discussed above, only saddle-type critical structures give rise to separatrices, and these separatrices have to be extracted in piecewise continuous vector fields, too.

4.2.2 Traditional Critical Structures within Discontinuities

As we have already seen, attracting sliding flow leads in forward time direction to a continuous vector field $\bar{\mathbf{u}}$, defined on the discontinuity. Correspondingly, repelling sliding flow leads in reverse time direction to a respective continuous vector field $\bar{\mathbf{u}}$, too. These vector fields are, by assumption, $(n-1)$ -dimensional, and exhibit traditional vector field topology in terms of critical structures and separatrices.

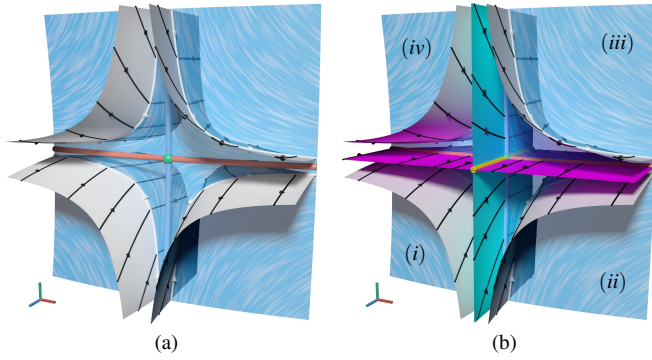


Fig. 4: (a) Attracting sliding flow (blue LIC) on discontinuity, with saddle-type critical point (green) and respective stable (blue) and unstable (red) manifolds. (b) Same as (a), with stable (cyan) and unstable (magenta) streamsets, induced by stable (blue) and unstable (red) manifold within sliding flow. Stable and unstable streamsets separate regions (i)–(iv) with qualitatively different streamset behavior (white). Streamsets extend to both sides of discontinuity (transparency).

The only saddle-type critical structure in 2D flow is the saddle, and it causes line-type separatrices (Figure 4a). Due to the uniqueness of $\bar{\mathbf{u}}$, these separatrices also separate respective streamsets *within* $\bar{\mathbf{u}}$ (white lines in Figure 4b). As a consequence, the streamsets (cyan and magenta surfaces in Figure 4b) seeded at these separatrices separate streamsets (white surfaces in Figure 4b) within the n -dimensional domain Ω . Notice that the red and blue separatrices represent a non-isotemporal section through the aimed streamsets. More important, such streamsets seeded at separatrices of $\bar{\mathbf{u}}$ represent separatrices of discontinuous vector field topology in nD space, i.e., they separate regions of Ω with qualitatively different streamset behavior.

We use blue and red color for traditional stable and unstable manifolds, respectively, which separate streamlines (1-manifold streamsets). On the other hand, stable and unstable streamset manifolds that separate streamsets which are not 1-manifold, are colored cyan and magenta, respectively. Finally, streamsets that are induced by saddle-type critical structures in $\bar{\mathbf{u}}$ are colored yellow. That is, we color the streamsets in Figure 4b that connect to stable line-type manifolds of $\bar{\mathbf{u}}$ cyan, those that connect to the unstable line-type manifolds of $\bar{\mathbf{u}}$ magenta, and those that connect to the saddle yellow. Notice that whereas traditional stable and unstable manifold require infinite integration time to reach a critical structure, stable and unstable streamset manifolds can reach them (as for the case in Figure 4b) in finite time, since they can “enter them from the embedding space”.

Periodic orbits in 2D flow (Figure 5a) cannot be of saddle-type, and thus do not give rise to separatrices within $\bar{\mathbf{u}}$. Nevertheless, since the periodic orbits themselves represent separating invariant sets in $\bar{\mathbf{u}}$, they also give rise to respective streamset separatrices. Attracting periodic orbits cause stable (cyan) streamset manifolds, whereas those streamsets that connect to repelling periodic orbits in $\bar{\mathbf{u}}$ are unstable (magenta). Thus, the cyan manifold in Figure 5b separates streamsets (white) in the interior from those in the exterior. Notice also the magenta streamset 1-manifolds connecting (in forward time) to the red spiral source at the center of this example.

4.2.3 Novel Structures

Although we defer topological structures induced by domain boundaries to future work, boundary switch curves (BSC), introduced by Weinkauff et al. [23] for continuous flow, come into play at discontinuities also within the domain. A traditional BSC represents a curve on the domain boundary that separates inflow from outflow. Thus, it consists of those points on the domain boundary where the vector field component normal to the boundary is zero. In other words, BSC can be obtained by zero-level isolines of the normal flow component on the boundary. A vector field defined on a continuous part Ω_i can exhibit BSC on its boundary $\partial\Omega_i$, i.e., on the discontinuities Σ_{ij} . In fact, slid-

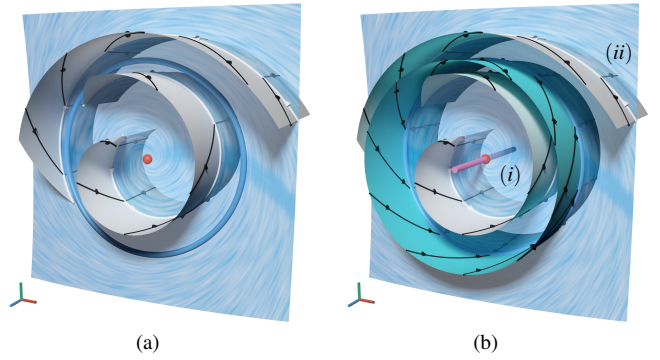


Fig. 5: (a) Attracting sliding flow (blue LIC) on discontinuity Σ_{ij} , with repelling focus (red) and attracting periodic orbit (blue curve). (b) Same as (a), with stable (cyan) streamset, induced by periodic orbit within discontinuity flow, and with unstable (magenta) streamset, induced by repelling focus. Stable streamset separates inner (i) from outer (ii) region with qualitatively different streamset behavior (white parts). Unstable streamset is of codimension 2 and thus not separating.

ing flow $\bar{\mathbf{u}}$ on codimension-1 discontinuities either reaches the domain boundary $\partial\Omega$, is limited by a BSC, or is limited by intersection with another discontinuity. Since discontinuities can act as critical structures, we consider their intersection an analog to higher-order topology [20], and because their intersection can take place in various configurations exceeding the scope of this paper, we address this as future work, too.

The boundary switch curves on discontinuities can either be inbound (Figures 2d and 6) or outbound (Figures 2e and 7). For piecewise continuous 2D flow, Figure 2 shows all basic topological cases (up to flow reversal) that are induced by the discontinuities themselves. Matching (congruent) BSC in the “left” and “right” part of a discontinuity would represent degenerate (not structurally stable) configuration in 2D. In piecewise continuous 3D flow, however, crossing BSC are stable unless they are congruent (see below).

First, we see that inbound BSC always induce separatrices (which consist of streamlines and separate streamlines, i.e., red in Figure 2d, red in Figure 6a, and blue in Figure 6b), whereas outbound BSC (Figures 2e and 7) do not. Second, we see that at an inbound BSC, streamsets undergo dimensional transition. For example, in areas (iii) and (iv) in Figure 2d, streamsets are two-dimensional, whereas they represent lines on the other side of the inbound BSC, where they are part of the red manifold. We call the violet manifolds in Figures 2e and 6 *equitrices*, since they separate regions with different manifoldness of equivalence streamset parts. In 3D flow (Figures 6a and 6b), equitrices are 2-manifolds, i.e., they are of codimension 1.

If we now revisit BSC-induced separatrices (e.g., red in Figure 2d), we identify the entire region ((iii) and (iv)) below the equitrices as belonging to the red separatrix, since this whole construct (streamset) separates the 1-manifold streamsets in region (i) from those in region (ii), and additionally since it flows into that separatrix. This property of BSC-induced separatrices also holds in 3D, i.e., they consist of a surface connected to the BSC in forward or reverse time, and a “wedge” volume connecting to the BSC from the other side, with the volume being delineated by the equitrix manifolds (Figure 6). As a consequence, inbound BSC on $\partial\Omega_i$ act as critical structures and give rise to separatrices. That is, they need to be extracted and used as seed curves for separatrices.

Let us now investigate crossing BSC in 3D piecewise continuous flow, i.e., both parts Ω_i and Ω_j exhibit a BSC on Σ_{ij} and these BSC intersect transversally, that is, are not congruent. Since there are two (inbound and outbound) types of BSC, their intersection leads to three combinations: inbound-inbound (Figures 8a, 8c and 8e), inbound-outbound (Figures 8b and 8d), and outbound-outbound (Figure 8f). The inbound-inbound configuration causes six regions, with regions (i), (ii), (iv), and (vi) containing 1-manifold streamsets, whereas region (v) (with attracting sliding flow) and region (iii) (with repelling

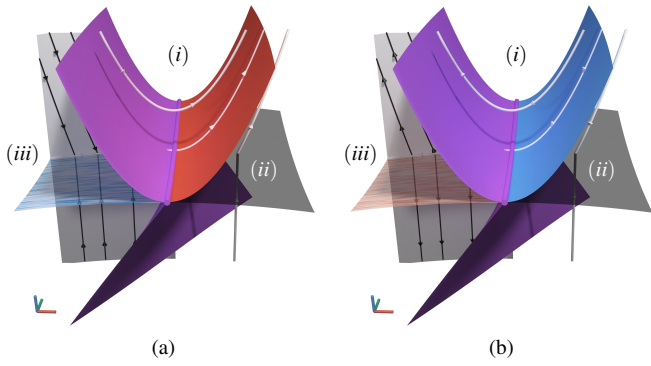


Fig. 6: Inbound boundary switch curves (violet lines) are bounding (a) attracting sliding flow (blue LIC) and (b) repelling sliding flow (red LIC). Selected streamset (white) is 2-manifold on the left of the boundary switch curve, and 1-manifold (and part of an unstable/stable manifold) on the right. Equitrices (violet surfaces) separate regions with 1-manifold ((i),(ii)) and 2-manifold (iii) streamset parts.

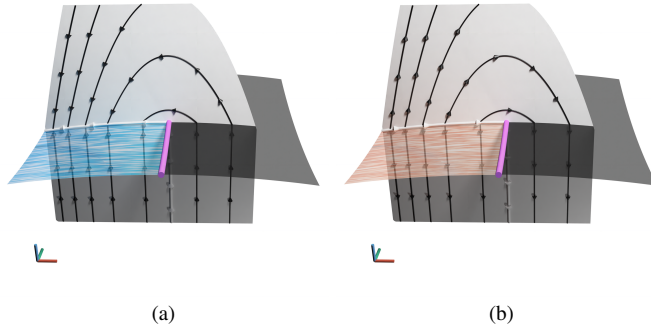


Fig. 7: Outbound boundary switch curves (violet) are bounding (a) attracting sliding flow (blue LIC) and (b) repelling sliding flow (red LIC). Entire space contains 2-manifold streamsets of qualitatively similar behavior, i.e., outbound BSC do not cause separatrices or equitrices.

sliding flow) contain 2-manifold streamsets. The equitrices (Figure 8c) separate the 1-manifold from the 2-manifold streamsets, whereas the stable and unstable manifolds (Figure 8a) separate 1-manifold streamsets with different behavior. The sliding flows involved in the inbound-inbound configuration exhibit hyperbolic sliding flow (resembling quadrants of 2D saddle flow).

In contrast, the inbound-outbound configuration always exhibits “rotating” sliding flow parts and splits the domain into three qualitatively different regions. The inbound BSC again gives rise to a stable/unstable manifold and an equitrix, but due to the interplay with the outbound BSC, half of the BSC generates a stable manifold, and the other half an unstable one (blue/red in Figure 8d). Notice that the 2-manifold streamset present at (i) is caused by the sliding flow at (ii), in other words, if a streamset would be seeded at a point on the discontinuity at (i), a 1-manifold streamset would originate. This is the explanation for the violet equitrix 2-manifold (iii) below the discontinuity, separating regions (iv) and (v).

Finally, intersection of two outbound BSC always exhibits an attracting and a repelling hyperbolic sliding flow similar to the inbound-inbound case, but does correspondingly neither cause stable/unstable manifolds nor equitrices (Figure 8f). However, since streamsets connected to one of the sliding flows also connect to the other sliding flow (see black curves in Figure 8f), this leads in general configurations to *dimensional blow up*, i.e., streamsets iteratively increase their dimension and eventually fill nD space in such configurations (semitransparent boundary of white 3-manifold streamset in Figure 8f). The reason for the dimensional blow up is that a 2-manifold streamset from one sliding flow in general reaches the other sliding flow in a transversal

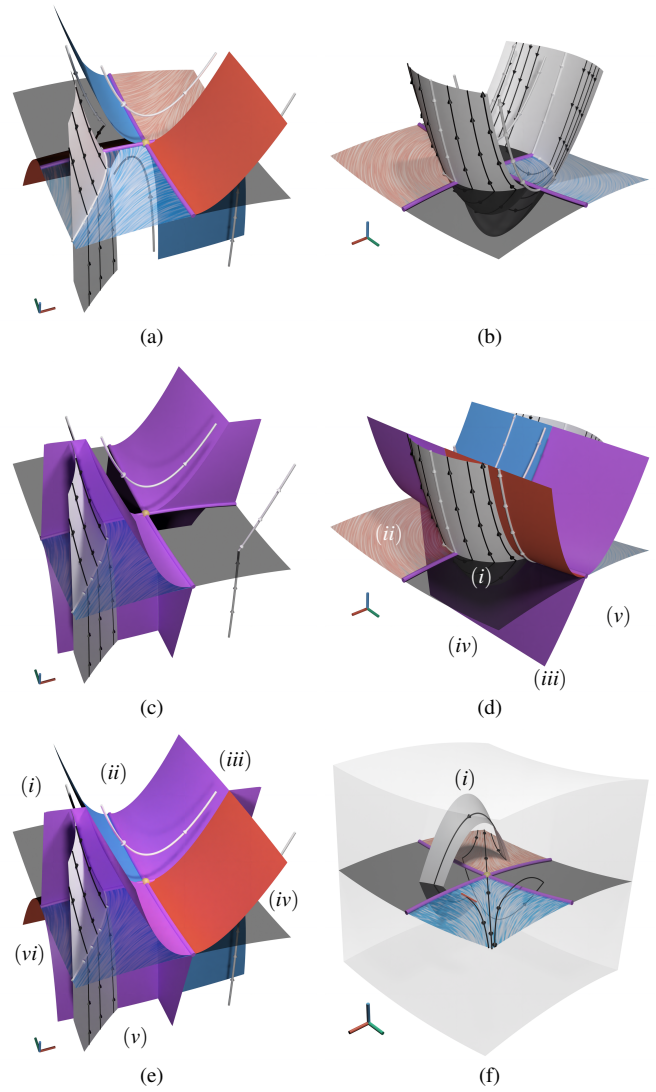


Fig. 8: (a),(c),(e) Intersection of two inbound boundary switch curves (BSC), with streamsets and stable/unstable manifolds (a), equitrices (c), and both (e). (b),(d) Intersection of inbound and outbound boundary switch curve, with streamset (b), and stable/unstable manifolds and equitrices (d). Intersection of two outbound BSC (f) does not exhibit manifolds or equitrices, since whole space is occupied by a single 3-manifold streamset (white) due to dimensional blow up.

manner. That is, the red intersection curve in Figure 8f between the 2-manifold streamset (part of it shown at (i)) and the attracting sliding flow does not match the 1-manifold streamsets (see LIC or part of black line) of the attracting sliding flow. Thus, this transversal intersection causes the streamset to grow iteratively between the two sliding flows to a 3-manifold due to the equivalence relation.

To summarize: Single-sided (non-intersecting) inbound BSC configurations cause one stable/unstable manifold and two equitrices. Single-sided (non-intersecting) outbound BSC do not give rise to topological structures. Two-sided (intersecting) BSC configurations give rise to stable and unstable manifolds as well as equitrices if an inbound BSC is involved. The outbound-outbound case does not give rise to topological structures.

4.2.4 Separatrix Bypassing

If, during integration, a stable or unstable manifold of the (traditional or novel) types defined above passes crossing flow, it simply exhibits C^0 continuity there. If, however, part of such a manifold reaches sliding flow in non-degenerate configuration, the sliding flow induces an

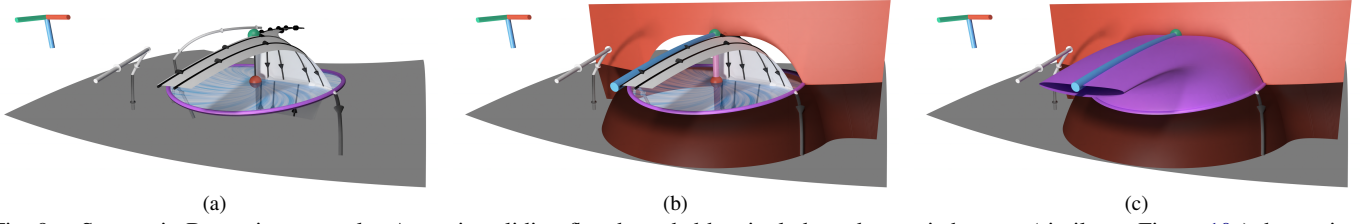


Fig. 9: Separatrix Bypassing example. Attracting sliding flow bounded by single boundary switch curve (similar to Figure 10a), bypassing the unstable manifold (red surface) of a 3D saddle (green). (a) 2-manifold streamset (white) converging in reverse time to 1D stable manifold (blue line in (b)) of the 3D saddle. (b) Sliding flow (blue LIC) bypasses red unstable manifold of saddle, causing respective hole in the unstable manifold (where the unstable manifold is not separating). (c) Equitrix (violet surface) represents boundary of region containing 2-manifold streamset parts. As a consequence, the intersection of the equitrix with the unstable manifold represents the boundary of separatrix bypassing.

equivalence streamset for each streamline of that part of the manifold, bypassing the separating property of that part of the manifold (Figure 9). Thus, those parts of traditional or novel stable and unstable manifolds that are on both sides of the manifold in contact with a streamset induced by themselves, do not separate streamsets and thus have to be removed from the stable or unstable manifold.

In fact, the interplay of separatrices in traditional topology can already become intricate. However, on the one hand, the additional dynamics induced by sliding flow increases complexity. On the other hand, sliding flow can erase parts of separatrices by bypassing. It has to be subject to further investigations to what extent these mechanisms balance each other.

4.3 Implementation

Unstructured grids lend themselves well for representing discontinuities by introduction of topological gaps, i.e., two cells that are geometrically adjacent along a face do not share the nodes of that face, i.e., replicate these nodes instead. Streamline integration in such configurations, however, depends on the specific implementation of the integrator. It is not uncommon for integrators to “bridge” topological and even geometrical gaps, e.g., to be able to trace streamlines across grids that rotate with respect to each other. Such skipping would in many cases also work if a single grid exhibits such topological gaps. That is, the integrator would jump from Ω_i to Ω_j , interpolate the value of \mathbf{u}_j there, and in case of attracting sliding flow this would bring integration back toward (and eventually across) the topological gap representing Σ_{ij} . Thus, straightforward application of integrators that are able to skip gaps would lead to a zigzag path along Σ_{ij} , and if the step size would be infinitesimal, this procedure could follow the sliding flow $\bar{\mathbf{u}}$ satisfactorily well. However, such infinitesimal integration step size is not feasible in practical applications.

Therefore, we developed an integrator that detects proximity to discontinuities (topological gaps) and in such cases directly integrates the sliding flow $\bar{\mathbf{u}}$. However, since detection of proximity to topological gaps is computationally expensive when determined directly on the unstructured grid, we additionally employ a preprocessing step that extracts the discontinuities as lower-dimensional (codimension-1) unstructured grids and samples $\bar{\mathbf{u}}$ on these grids. During integration, we determine proximity to this type of discontinuity representation by computing the shortest distance between the current integration position and the lower-dimensional unstructured grids, and by testing if this distance is within a user-defined threshold δ_{tol} . If it is, we continue (or enter) sliding flow integration mode. If it is not, we continue (or enter) regular integration of \mathbf{u} .

Our custom integrator is based on the fourth-order Runge–Kutta scheme with constant step size. To ensure stability, δ_{tol} has to be chosen larger than the integration step. In our experiments, a factor of 2 provided stable integration.

5 RESULTS

We evaluate and demonstrate our approach using a set of examples of increasing complexity.

5.1 Unbounded Attracting Sliding Flow

The probably simplest example involving sliding flow is obtained by an attracting discontinuity with approximately uniform flow. To demonstrate the versatility of our approach and to avoid degeneracies, we employ an overall deformation, leading to non-planar discontinuity Σ_{ij} . This example has been used for introducing equivalence classes and streamsets in Figure 3 and Section 4.1.

First, we defined the following vector field on $\Omega_{z < 0}$ and $\Omega_{z > 0}$

$$\mathbf{u}(\mathbf{x}) = \begin{cases} (2 + \cos(fx), mx, 1)^\top & \text{if } z < 0, \\ (2 + \cos(fx), mx, -1)^\top & \text{if } z > 0, \end{cases} \quad (24)$$

with frequency $f = 2.5$ and $m = -0.5$. After sampling the data on a uniform grid of $30 \times 30 \times 30$ cells with topological gap aligned with $z = 0$, we applied a perturbation smaller than the cell length to obtain a curvilinear grid (as we did for all basic examples). This deformation is given by the following polynomial function of degree two: $\boldsymbol{\mu}(\mathbf{x}) = (0, 0, -0.005x^2 + 0.005y^2)^\top$.

5.2 Saddle

The Saddle dataset (Figure 4 and Section 4.2.2) consists of a 2D saddle-type flow on the discontinuity, with additional attracting component toward the discontinuity. The field is defined as follows

$$\mathbf{u}(\mathbf{x}) = \begin{cases} (x, 0, 1)^\top & \text{if } z < 0, \\ (0, -y, -1)^\top & \text{if } z > 0, \end{cases} \quad (25)$$

and has also been sampled on a grid with $30 \times 30 \times 30$ cells with topological gap aligned with $z = 0$ and the same subsequent deformation.

5.3 Periodic Orbit

The Periodic Orbit dataset (Figure 5) exhibits an attracting 2D periodic orbit in attracting sliding flow, with a repelling focus at its center:

$$\mathbf{u}(\mathbf{x}) = \begin{cases} (0, 0, 1)^\top & \text{if } z < 0, \\ (s(x, y)x - y, x + s(x, y)y, -1)^\top & \text{if } z > 0, \end{cases} \quad (26)$$

with $s(x, y) = -2(1 + e^{-r(x, y)+1})^{-1}$ and $r(x, y) = \sqrt{x^2 + y^2}$, sampled on a grid with $30 \times 30 \times 30$ cells with topological gap aligned with $z = 0$ and the same subsequent deformation. See also Section 4.2.2.

5.4 Boundary Switch Flow

Again sampled on a grid $30 \times 30 \times 30$ cells with topological gap aligned with $z = 0$ and the same subsequent deformation, the inbound Boundary Switch Flow (Figure 6) is defined as

$$\mathbf{u}(\mathbf{x}) = \begin{cases} (0, 1, -3y)^\top & \text{if } z < 0, \\ (1, 0, 3x)^\top & \text{if } z > 0, \end{cases} \quad (27)$$

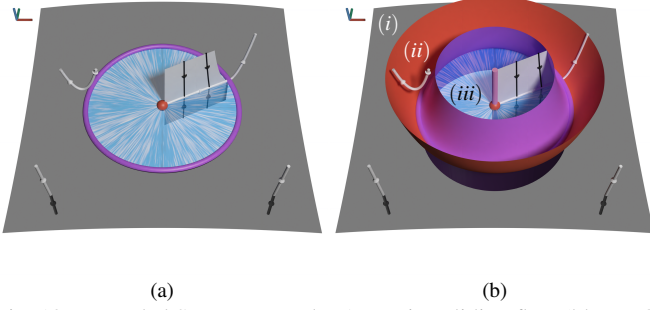


Fig. 10: Bounded Source example. Attracting sliding flow (blue LIC) with 2D repelling node (red point), bounded by closed inbound boundary switch curve (violet line). (a) Streamset (white) changes dimensionality when crossing the boundary switch curve. (b) Unstable manifold (red surface) and equitrices (violet surfaces) reveal regions (i) and (ii) containing 1-manifold streamset parts with qualitatively different behavior, and region (iii) containing 2-manifold streamset parts.

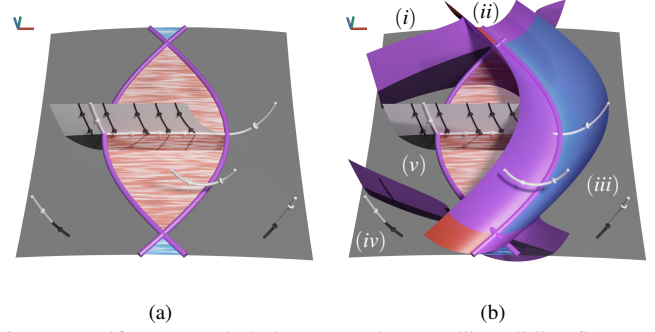


Fig. 11: Uniform Bounded Flow example. Repelling sliding flow (red LIC), bounded by outbound (left) and inbound (right) boundary switch curve (violet lines). (a) While dynamics in sliding flow is somewhat similar to Figure 10a, the induced streamsets (white) exhibit strong asymmetry due to opposite type of BSC. (b) 2-manifold streamset parts in region (v) bounded by equitrices, and 1-manifold streamset parts in regions (i)–(iv) separated by stable/unstable manifolds.

and the outbound one (Figure 7) as

$$\mathbf{u}(\mathbf{x}) = \begin{cases} (-0.5y, 0, 1)^\top & \text{if } z < 0, \\ (-1, 0, 3x)^\top & \text{if } z > 0. \end{cases} \quad (28)$$

See Section 4.2.3 for a discussion of these two examples.

5.5 Bounded Source

The Bounded Source example (Figure 10) represents the simplest bounded sliding flow example and is defined by

$$\mathbf{u}_2(\mathbf{x}) = \begin{pmatrix} x \\ y \\ x^2 + y^2 - 1 \end{pmatrix} \quad (29)$$

and $\mathbf{u}_1(\mathbf{x}) = (0, 0, d)^\top$ for $d = 1$, with discretization $60 \times 60 \times 30$ and same deformation. In general, we chose $\mathbf{u}_1(\mathbf{x})$ to be normal to the discontinuity, since this causes the resulting flow on the discontinuity to be the orthogonal projection of $\mathbf{u}_2(\mathbf{x})$ onto the discontinuity, which leverages the creation of these cases. The component of $\mathbf{u}_2(\mathbf{x})$ that is normal to the discontinuity was chosen to create a circular BSC around the center of the discontinuity. A single source can be bounded by a single BSC, since it exhibits only outflow across the BSC.

As seen in Figure 10a, a 2D repelling focus critical point (red point) with respective streamset (magenta) is located at the center of the discontinuity. Right to it, a streamset leaves the discontinuity through an inbound BSC, where the 2-manifold streamset is compressed into a 1-manifold one that is part of the red separatrix in Figure 10b.

5.6 Uniform Bounded Flow

Uniform sliding flow can only be bounded by an inbound and an outbound BSC, due to the involved boundary restrictions. Observe in Figure 1 that when an inbound BSC and an outbound BSC intersect, the discontinuity changes from attracting to repelling and vice versa. We can see in Figure 11b that an outbound BSC (left arc) indeed does not separate streamsets. However, the streamset is 2-manifold in the interior (v) and merges into a 1-manifold streamset at the inbound BSC to the right (iii). Furthermore, the streamline at the bottom left (iv) in Figure 11b is separated from the streamset through an equitrix, and the one at the bottom right (iii) by the stable manifold of the BSC. The flow is given by

$$\mathbf{u}(\mathbf{x}) = \begin{cases} (1 - z, 0, 4(x + \cos(y) - 0.3))^\top & \text{if } z < 0, \\ (1 - z, 0, 4(x - \cos(y) + 0.3))^\top & \text{if } z > 0, \end{cases} \quad (30)$$

again with discretization $60 \times 60 \times 30$ and same deformation.

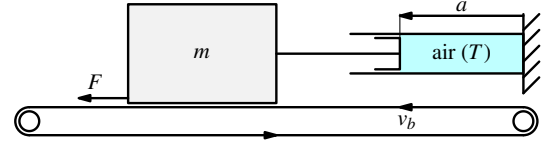


Fig. 12: Dry Friction example. Block of mass m , driven by friction force F caused by interaction with belt moving at velocity v_b , and interacting with air spring (light blue) at temperature T .

5.7 Separatrix Bypassing

The bypassing example (Figure 9) is defined as follows:

$$\mathbf{u}(\mathbf{x}) = \begin{cases} (0.5\alpha x, -2\alpha \min(|z|, 1)y, z + 0.5)^\top & \text{if } z < 0, \\ (x - y, x + y, (x^2 + y^2)|z|^\beta)^\top & \text{if } z > 0, \end{cases} \quad (31)$$

with $\alpha = 0.5$ and $\beta = 0.01$, and again discretization $30 \times 30 \times 30$ and same deformation. Please see Section 4.2.4 for a discussion.

5.8 Dry Friction

Dry friction is the force that arises from one solid surface sliding on another solid surface. When an exterior force acts on a solid body resting on a solid surface, it has to overcome static friction to enable relative movement. Once the solid starts moving, it experiences kinetic friction. The transition from resting to relative motion is assumed to be instantaneous and discontinuous. Therefore, the motion of an object experiencing dry friction can be described by a Filippov system.

One such system can be found in a rolling band setup depicted in Figure 12. In this setup, a solid block is lying on a rolling band that is connected to an air spring. A similar setup with a spring (resulting in a 2D phase space) can be found in the work of Leine [17], which served as the basis for our model with air spring and thus 3D phase space.

Let $\mathbf{x} = (a, \dot{a}, T)^\top$ be a point in phase space that describes the system's state, where a is the deflection of the spring, \dot{a} its rate of change, and T the temperature of the air inside the air spring. Then we can formulate the motion of the block in terms of a differential equation

$$\dot{\mathbf{x}} = \begin{pmatrix} \dot{a} \\ \frac{-k(T)}{m}a + \frac{F(a, v_{rel})}{m} \\ g(\mathbf{x}) \end{pmatrix}, \quad (32)$$

$$F(a, v_{rel}) = \begin{cases} \min(|k(T)a|, F_s) \operatorname{sgn}(k(T)a) & \text{if } v_{rel} = 0, \\ -\frac{F_s \operatorname{sgn}(v_{rel})}{1 + \delta|v_{rel}|} & \text{if } v_{rel} \neq 0, \end{cases} \quad (33)$$

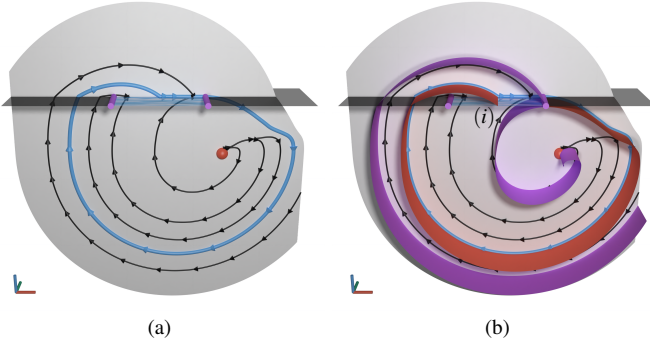


Fig. 13: Phase space of a temperature-independent dry friction case (extruded/invariant along T -axis), with attracting sliding flow (blue LIC) bounded by outbound (left) and inbound (right) boundary switch curve (violet curves) (a -axis red, \hat{a} -axis blue, T -axis green). (a) Attracting periodic orbit (blue line) revolves around 2D repelling focus (red point). (b) Unstable manifold (red surface) and equitrices (violet surfaces) are spiraling around the repelling focus.

where m is the mass of the block, $k(T)$ the temperature-dependent air spring constant, v_{rel} the relative velocity of the block to the moving band, $g(\cdot)$ a function describing the change of temperature, $F(\cdot)$ the total friction force, and F_s the static friction force.

In the first dry friction case, we assume the system to be independent of the temperature T , i.e., $k(T) = k_0$ for some constant k_0 and $g(\mathbf{x}) = 0$ everywhere. We use $F_s = 1.2\text{N}$, $\delta = 4\text{s/m}$, $k_0 = 1\text{N/m}$, $m = 1\text{kg}$, and let the band move at constant speed $v_b = 0.2\text{m/s}$. This leads to the extrusion shown in Figure 13. Trajectories entering the attracting sliding flow (blue LIC) imply the transition from sliding contact to static contact of the block with the band, while trajectories going through the crossing flow mean, that the block skipped static contact. The discontinuity exhibits an outbound (left) and inbound (right) BSC, from the latter of which an unstable manifold and two equitrices follow. The separatrix reenters the discontinuity at (i) and then leaves the discontinuity through the inbound BSC. This results in a periodic orbit (blue streamline), which is stable in this case, and since trajectories on the discontinuity can intersect the periodic orbit in finite time, the block will always enter this periodic motion after a finite time, no matter the initial conditions except for the repelling focus (red point). One equitrix spirals out of the system, while the other converges toward a repelling focus in reverse time. Therefore, in reverse time, the separatrix separates streamlines that spiral out of the system from those that converge to the repelling focus.

For our second case, we used $F_s = 1.8\text{N}$ and introduce a temperature-dependent spring constant

$$k(T) = \frac{1}{1 + e^{(-T)}}(k_1 - k_0) + k_0, \quad (34)$$

where we set $k_1 = 4\text{N/m}$. We further assume that

$$g(\mathbf{x}) = -c(T - T_0), \quad (35)$$

where $c = 0.6\text{1/s}$ is a heat loss coefficient and $T_0 = -1\text{K}$ is the equilibrium temperature of the system. Equation 35 returns the system to $T = T_0$, while Equation 34 models the transition of the air spring between different spring constants. The spring constant of the air spring increases with increasing temperature.

The phase space is shown in Figure 14a, with similar structure to Figure 13. Since the temperature converges toward T_0 due to heat loss, this results in a 3D spiral saddle (green point) and a stable periodic orbit (blue streamline) located on the separatrix for $T = T_0$. As can be seen in Figure 14a, streamsets spiral toward the periodic orbit.

6 DISCUSSION

While having demonstrated the utility of streamset-based vector field topology for non-unique flow, our current approach exhibits limita-

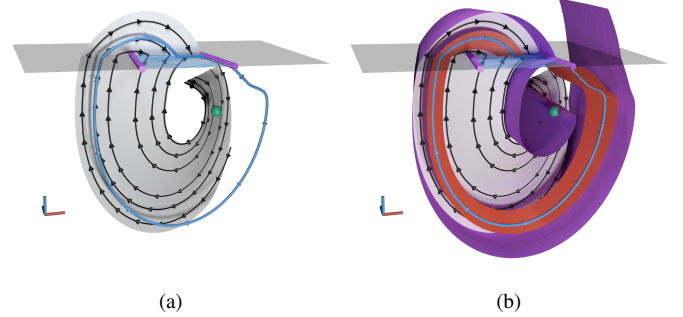


Fig. 14: (a) Temperature-dependent dry friction model. Trajectories converge toward the periodic orbit, which is the cross section of the red unstable manifold at the equilibrium temperature. (b) Similar to Figure 13b, unstable manifold and equitrices are not separating.

tions and shortcomings. Firstly, our description is incomplete without considering effects induced by the domain boundary $\partial\Omega$. Boundaries and discontinuities have a lot in common, and we expect additional topologically relevant structures from their interplay.

Another important aspect is dimensional blow up, i.e., the increase in dimensionality when a streamset induced by one discontinuity intersects with another discontinuity, which in turn induces another streamset. Due to the transitivity of the equivalence class, the resulting structure must be equivalent in every point across both streamsets, resulting in a n -dimensional object. While having demonstrated this effect in Section 4.2.3, approaches have to be developed to efficiently obtain the boundary of these n -dimensional objects. Furthermore, their bypassing is to be investigated.

Regarding the implementation, our extraction scheme can be improved in terms of balancing robustness against efficiency. While our current approach works well in simple cases, it would be necessary to optimize it to efficiently handle complex configurations, especially in the presence of close-to-degenerate configurations and noise.

7 CONCLUSION

In this work, we extended the concept of vector field topology to piecewise continuous vector fields exhibiting codimension-1 discontinuities. To account for the transport non-uniqueness induced by the discontinuities, we introduced a time-reversible flow equivalence relation, which enabled us to formulate streamsets, a generalization of streamlines for piecewise continuous flow. Based on these streamsets, we examined the role of traditional (continuous) vector field topology in discontinuous flow, and additionally identified novel critical structures and their induced manifolds, providing the aimed discontinuous vector field topology. Besides separating structures, we also identified the necessity of introducing manifolds that separate streamset parts of different dimensionality. Our implementation models discontinuities in vector fields using topological gaps in unstructured grids, which enables utilization of existing visualization frameworks and formats.

We observed various unexpected and challenging phenomena in discontinuous vector field topology. While we were able to investigate separatrix bypassing and dimensional blow up, we identified, among others, the need to include the domain boundaries and to address the higher-order counterpart of intersecting discontinuities, whose investigation, however, exceeded the scope of this paper.

Our research has several potential avenues for future exploration and extension. These include the consideration of domain boundaries, intersecting discontinuities, time-dependent vector fields, higher-dimensional streamsets, and the incorporation of non-smooth bifurcation theory. By investigating these areas, one could obtain a deeper understanding of the behavior of discontinuous and non-unique complex systems in various domains, including physics, biology, and engineering. Last but not least, we expect our streamset concept to be useful in the analysis of other domains that exhibit non-uniqueness of transport.

ACKNOWLEDGMENTS

This work is supported by Deutsche Forschungsgemeinschaft (DFG) under Germany's Excellence Strategy EXC-2181/1 - 390900948 (the Heidelberg STRUCTURES Excellence Cluster) and under Project-ID 281071066 – TRR 191 (Transregional Collaborative Research Center SFB / TRR 191).

REFERENCES

- [1] A. A. Andronov. Systems grossiers. *Dokl. Acad. Nauk SSSR*, 14:247–251, 1937. 2
- [2] D. Asimov. Notes on the topology of vector fields and flows. Technical report, NASA Ames Research Center, RNR-93-003, 1993. 2
- [3] J. M. Ball. Continuity properties and global attractors of generalized semi-flows and the Navier–Stokes equations. *Journal of Nonlinear Science*, 7(5):475–502, 1997. 2, 4
- [4] B. Cabral and L. C. Leedom. Imaging vector fields using line integral convolution. In *Proceedings of the 20th Annual Conference on Computer Graphics and Interactive Techniques*, pages 263–270, 1993. 4
- [5] S. Fernández-García, D. A. García, G. O. Tost, M. di Bernardo, and M. R. Jeffrey. Structural stability of the two-fold singularity. *SIAM Journal on Applied Dynamical Systems*, 11(4):1215–1230, 2012. 2
- [6] A. F. Filippov. *Differential Equations with Discontinuous Righthand Sides*, volume 18. Springer Netherlands, 1988. 2, 3
- [7] P. Glendinning and M. R. Jeffrey. *An Introduction to Piecewise Smooth Dynamics*. Advanced Courses in Mathematics - CRM Barcelona. Springer International Publishing, 2019. 2, 3
- [8] J. L. Helman and L. Hesselink. Representation and display of vector field topology in fluid flow data sets. *IEEE Computer*, 22(8):27–36, 1989. 1
- [9] J. L. Helman and L. Hesselink. Visualizing vector field topology in fluid flows. *IEEE Computer Graphics and Applications*, 11(3):36–46, 1991. 1
- [10] L. Hofmann, B. Rieck, and F. Sadlo. Visualization of 4D vector field topology. *Computer Graphics Forum*, 37(3):301–313, 2018. 2
- [11] L. Hofmann and F. Sadlo. Extraction of distinguished hyperbolic trajectories for 2D time-dependent vector field topology. *Computer Graphics Forum*, 39(3):303–315, 2020. 1
- [12] L. Hofmann and F. Sadlo. Local extraction of 3D time-dependent vector field topology. *Computer Graphics Forum*, 40(3):111–122, 2021. 1
- [13] M. R. Jeffrey. Hidden dynamics in models of discontinuity and switching. *Physica D: Nonlinear Phenomena*, 273–274:34–45, 2014. 2
- [14] M. R. Jeffrey. Hidden dynamics of dry-friction oscillators. page 10. Proc. of ICoEV Ljubljana, 2015. 2, 3
- [15] M. R. Jeffrey. Hidden degeneracies in piecewise smooth dynamical systems. *International Journal of Bifurcation and Chaos*, 26(05):1650087, 2016. 3
- [16] M. R. Jeffrey. *Hidden Dynamics: The Mathematics of Switches, Decisions and Other Discontinuous Behaviour*. Springer International Publishing, 2018. 2, 3
- [17] R. Leine. *Bifurcations in discontinuous mechanical systems of Filippov-type*. Phd thesis, Technische Universiteit Eindhoven, 2000. 8
- [18] V. S. Melnik and J. Valero. On attractors of multivalued semi-flows and differential inclusions. *Set-Valued Analysis*, 6(1):83–111, 1998. 2, 4
- [19] M. Otto, T. Germer, H.-C. Hege, and H. Theisel. Uncertain 2D vector field topology. *Computer Graphics Forum*, pages 347–356, 2010. 1
- [20] G. Scheuermann, H. Hagen, H. Krüger, M. Menzel, and A. Rockwood. Visualization of higher order singularities in vector fields. In *Proceedings IEEE Visualization*, pages 67–74, 1997. 2, 5
- [21] H. Theisel, T. Weinkauff, H.-C. Hege, and H.-P. Seidel. Saddle connectors - an approach to visualizing the topological skeleton of complex 3D vector fields. In *Proc. IEEE Conference on Visualization*, pages 225–232, 2003. 1
- [22] C. Thieme. Multiflows: A new technique for Filippov systems and differential inclusions. arXiv:1905.07051, 2019. 2, 4
- [23] T. Weinkauff, H. Theisel, H.-C. Hege, and H.-P. Seidel. Boundary switch connectors for topological visualization of complex 3D vector fields. In *Proc. Eurographics / IEEE VGTC Symposium on Visualization*, pages 183–192, 2004. 1, 5